Acta Crystallographica Section A
Foundations of Crystallography
ISSN 0108-7673

Received 8 January 2009
Accepted 14 April 2009

Formation of interference fringes in the Bragg–(Bragg)^m–Laue mode

Kenji Hirano,[a]* Tomoe Fukamachi,[a] Masami Yoshizawa,[a] Riichirou Negishi,[a] Keiichi Hirano[b] and Takaaki Kawamura[c]

[a]Saitama Institute of Technology, 1690 Fusaiji, Fukaya, Saitama 369-0293, Japan, [b]Institute of Material Structure Science, KEK-PF, High Energy Accelerator Research Organization, Oho-machi, Tukuba, Ibaraki 305-0801, Japan, and [c]Department of Mathematics and Physics, University of Yamanashi, Kofu, Yamanashi 400-8510, Japan. Correspondence e-mail: q6006qqp@sit.jp

X-ray interference fringes in the beams diffracted from a lateral surface of a thin plane-parallel crystal are measured and analyzed using Wagner's approach [Wagner (1956), *Z. Phys.* **146**, 127–168]. It is found that the fringes are caused by the interference between the internal waves excited by the incident beam in both the Bragg–Laue case and the Bragg–Bragg–Laue case. The period of the interference fringes is shown to be proportional to the distance between the incident point of the X-ray and the crystal edge, and to be inversely proportional to the crystal thickness.

1. Introduction

X-ray interference fringes in the diffraction from a lateral surface (we call this diffraction DLS for brevity) were recently measured from a thin plane-parallel crystal in the Bragg–(Bragg)^m–Laue (BB^{m}L) geometry (Fukamachi *et al.*, 2004, 2005). The first 'Bragg' means the initial diffraction is in the Bragg case, '(Bragg)^m' means a sequence of m diffractions in the Bragg case between the top and bottom surfaces, and 'Laue' means the final diffraction in the Laue case from the lateral surface as shown in Fig. 1. In this figure, H is the crystal thickness and L is the distance between the incident point of the X-ray and the crystal edge. The intensities P'_h and P'_t mean the Laue diffraction in the diffracted and transmitted directions from the lateral surface, respectively. Yan & Noyan (2005) have also observed DLS in the BB^{m}L case using both white and monochromatic X-rays. Since DLS is produced when the linear absorption coefficient μ is minimized due to the dynamical diffraction (Borrmann) effect, the path length of the X-rays is quite large.

In this paper we report on the measurements of the interference fringes in the BB^{m}L case (m = 0 and 1) using X-rays from synchrotron radiation and the analysis of the fringes using Wagner's approach (Wagner, 1956), which is based on Laue's dynamical theory of diffraction.

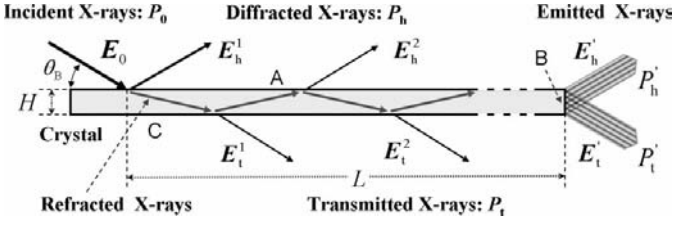

Figure 1
Schematic illustration of the beam geometry in the BB^{m}L case. θ_B is the Bragg angle, H is the crystal thickness and L is the distance between the incident point of the X-ray and the edge of the crystal.

2. Experiment

The measuring system is schematically shown in Fig. 2. The experiments were carried out using X-rays from synchrotron radiation at BL-15C, Photon Factory, KEK, Tsukuba, Japan. The DLS of the 220 reflection was observed from a Ge crystal whose etch-pit density was less than 500 cm^{-2} and thickness H was 45 $\pm$ 2 µm. The X-rays were σ-polarized and were monochromated using an Si 111 double-crystal monochromator and a Ge 220 monochromator. The X-ray energy was 11100 $\pm$ 0.5 eV, which was 3 eV below the Ge K-

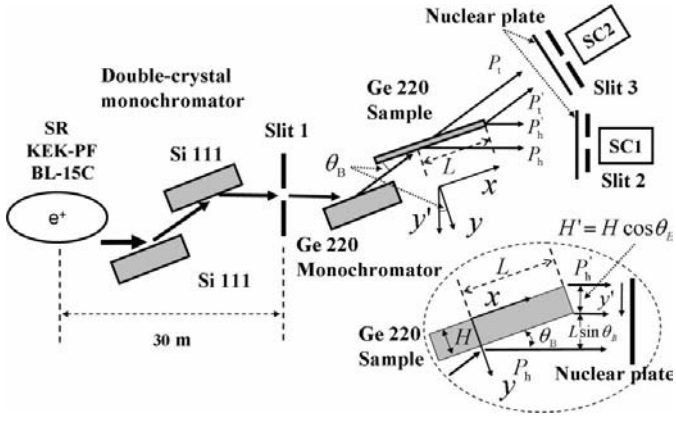

Figure 2
Schematic diagram of the measuring system. SR is the synchrotron-radiation X-ray source and SC is the scintillation counter. The crystal thickness of the specimen is 45 $\pm$ 2 µm. The inset is a magnification of the region around the sample crystal.

Table 1
Periods of the interference fringes.

	Λ_B (μm)		
L (μm)	Measured	Calculated using equation (5)	Calculated using equation (17)
576 ± 40	8.1 ± 0.8	8.1	8.1
657 ± 40	9.8 ± 1.0	9.4	9.4
801 ± 40	12.1 ± 1.2	12.3	11.7

absorption edge and the absorption effect is small. The divergence angle of the incident beam was approximately 5 arcsec, which was estimated by the full width at half-maximum (FWHM) of the Ge 220 reflection. The vertical and horizontal widths of the incident beam after slit 1 were adjusted to be 20 and 500 μm, respectively. The transmitted (P_t) and diffracted (P_h) intensities as well as the emitted beam intensities from the lateral surface in the transmitted (P_t') and diffracted (P_h') directions were recorded on the nuclear plates and were measured by scintillation counters. Fig. 3(*a*) shows a photograph of the diffraction patterns of P_t (upper) and P_t' (lower) and Fig. 3(*b*) shows those of P_h (lower) and P_h' (upper) when the incident angle is set to the value at which the intensities of P_h' and P_t' become maximum. The interference fringes are observed in the patterns of P_h' and P_t'.

Fig. 4 shows the intensity distributions of P_h' (filled circles) and P_t' (open circles) with respect to the position (y) in the photograph of Fig. 3. The distance L is changed; L is 576 ± 40 μm in Fig. 4(*a*), 657 ± 40 μm in (*b*) and 801 ± 40 μm in (*c*). The backgrounds of P_h' are lower than those of P_t'. The intensity variations of P_h' and P_t' with respect to the position are in phase with each other regardless of the distance L. The peak at $y = H$ is not due to the interference, as described later.

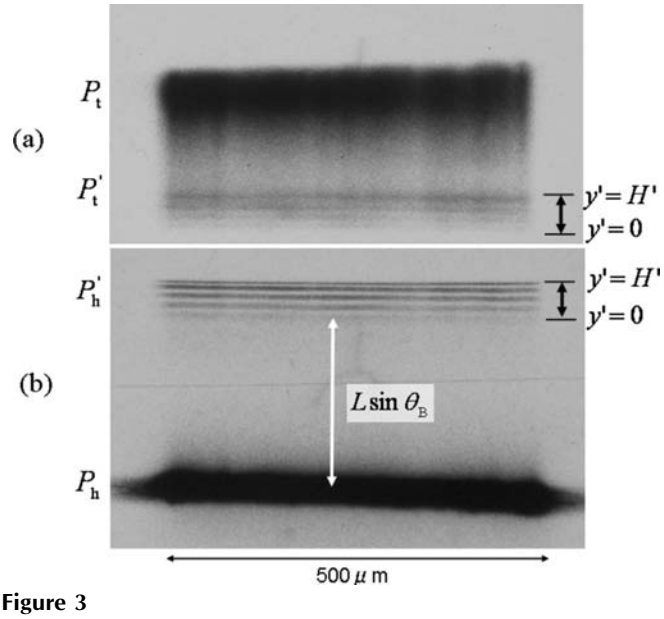

Figure 3
Photographs of P_t and P_t' (*a*), and P_h and P_h' (*b*). In (*a*) the upper part is P_t and the lower part is P_t'. In (*b*) the upper part is P_h' and the lower part is P_h. The distance L is 801 μm. Here $y' = y \cos\theta_B$ and $H' = H \cos\theta_B$ as shown in Fig. 2.

The period of the interference fringes Λ_B increases linearly as L increases. The periods of the interference fringes between the first and the second peaks from $y = H$ in P_h' were measured for the three values of L and are listed in Table 1.

3. Analysis of interference fringes

3.1. Propagating direction of X-ray energy

It is well known that the propagating direction of the X-ray energy in a crystal corresponds to the direction of the corresponding Poynting vector. It is expressed by using the electric displacement fields $\mathbf{D}_0^{(j)}$ of the transmitted (0) beam and $\mathbf{D}_h^{(j)}$ of the hth diffracted beam. The superscript (j) on $\mathbf{D}$ represents the dispersion surface (1) or (2). The time- and space-averaged Poynting vector $\mathbf{S}^{(j)}$ is given by

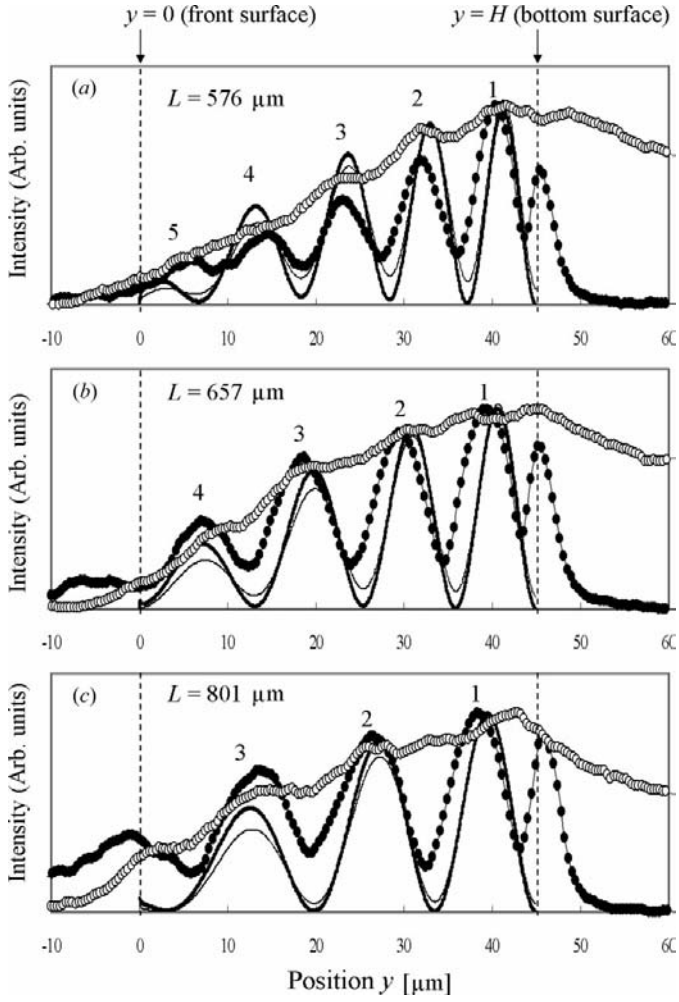

Figure 4
The DLS intensities of the Ge 220 reflection with respect to the crystal thickness. The filled circles show the measured intensities of P_h' and the open circles those of P_t'. The thick solid lines show the calculated intensity of P_h' and the thin solid lines show P_t' with respect to the crystal thickness. The distance L is (*a*) 576 ± 40 μm (*b*) 657 ± 40 μm and (*c*) 801 ± 40 μm. In the calculation, the normal atomic scattering factor of 22.37, the real part of anomalous scattering factor of −9.08 and the imaginary part of 1.13 are used (Yoshizawa *et al.*, 2005).

$$\mathbf{S}^{(j)} = \mathbf{s}_0|\mathbf{D}_0^{(j)}|^2 + \mathbf{s}_h|\mathbf{D}_h^{(j)}|^2 + (\mathbf{s}_0 + \mathbf{s}_h)|\mathbf{D}_0^{(j)}||\mathbf{D}_h^{(j)}|\cos\varphi^{(j)}, \quad (1)$$

as shown in Fig. 5. Here $\mathbf{s}_0$ and $\mathbf{s}_h$ are the unit vectors of the transmitted and diffracted beam directions, respectively, and the phase $\varphi^{(j)}$ is defined by

$$\varphi^{(j)} = \arg(\mathbf{D}_h^{(j)}) - \arg(\mathbf{D}_0^{(j)}). \quad (2)$$

In a non-absorbing crystal, the third term of the right side of (1) can be neglected as $\cos\varphi^{(j)} = 0$. Then the Poynting vector $\mathbf{S}^{(j)}$ is written as

$$\mathbf{S}^{(j)} = \mathbf{s}_o|\mathbf{D}_0^{(j)}|^2 + \mathbf{s}_h|\mathbf{D}_h^{(j)}|^2. \quad (3)$$

The angle $\varepsilon^{(j)}$ between the Poynting vector and the diffraction plane is given by

$$\tan\varepsilon^{(j)}\cot\theta_B = \frac{|\mathbf{D}_0^{(j)}|^2 - |\mathbf{D}_h^{(j)}|^2}{|\mathbf{D}_0^{(j)}|^2 + |\mathbf{D}_h^{(j)}|^2} = \frac{1 - [r^{(j)}]^2}{1 + [r^{(j)}]^2}, \quad (4)$$

where $r^{(j)} = |\mathbf{D}_h^{(j)}/\mathbf{D}_0^{(j)}|$ is the reflectivity and θ_B is the Bragg angle (Pinsker, 1978). Hereafter, we drop the superscript j on ε, φ, r and the Poynting vector $\mathbf{S}$.

3.2. Interference fringes

We study the origin of the interference fringes observed in DLS by using Wagner's approach (Wagner, 1956). Fig. 6 shows the dispersion surface for a weakly absorbing crystal in the upper part and the effective absorption coefficient μ in the lower part for the X-ray energy corresponding to the present experiment. The parameter W is defined by $W = X/X_0$ with $X_0 = 1/(2\Lambda)$, $\Lambda = \lambda\cos\theta_B/|\chi_h|$, where λ is X-ray wavelength and χ_h is the hth Fourier transform of the X-ray polarizability. The width $\Delta|W|$ of the DLS beam can be estimated to be approximately 0.1. This width corresponds to the angle width of 0.25 arcsec for the Ge 220 reflection.

In the present experiment, since the incident divergence angle is 5 arcsec and the incident beam is regarded as a spherical wave, the two beams corresponding to $\mathbf{S}_{m=0}$ and $\mathbf{S}'_{m=0}$ are simultaneously excited, as shown in Figs. 6 and 7. The beams corresponding to $\mathbf{S}_{m=0}$ in the angle region $\varepsilon \le \varepsilon_1 = \tan^{-1}(H/L)$ directly reach the lateral surface B (BL case) as shown in Fig. 7. The beams corresponding to $\mathbf{S}'_{m=0}$ in the region $\varepsilon > \varepsilon_1$ reach the bottom surface C first, parts of the beams are reflected to the beams corresponding to $\mathbf{S}'_{m=0}$ which reach the surface B (BBL case), and the rest of them are transmitted through the bottom surface. The incident beam whose electric field is $\mathbf{E}_0$ induces two electric displacement fields $\mathbf{D}_0^{1(1)}$ and $\mathbf{D}_h^{1(1)}$ at a tie point on the dispersion surface (1). The Poynting vectors of $\mathbf{S}_{m=0}$ and $\mathbf{S}'_{m=0}$ are consistent with $\mathbf{D}_0^{1(1)}$ and $\mathbf{D}_h^{1(1)}$. As described above, the beams corresponding to $\mathbf{S}_{m=0}$ directly reach the point y_0 on the surface B. The beams corresponding to $\mathbf{S}'_{m=0}$ consistent with the two electric displacement fields $\mathbf{D}_0^{1(2)}$ and $\mathbf{D}_h^{1(2)}$ excited at a tie point on the dispersion surface (2) also reach the point y_0 on the surface B. At the point y_0, there are two components $\mathbf{D}_h^{1(1)}(y_0)$ and $\mathbf{D}_h^{1(2)}(y_0)$ [$\mathbf{D}_0^{1(1)}(y_0)$ and $\mathbf{D}_0^{1(2)}(y_0)$] in the diffracted [transmitted] beam direction. The intensities P'_h and P'_t at y_0 are given by

$$P'_h(y_0) = \left|\Omega_{BL}\mathbf{D}_h^{1(1)}\exp\left[-i2\pi\left(k_{hY}^{(1)}y_0 + k_{hX}^{(1)}L\right)\right] + \Omega_{BBL}\mathbf{D}_h^{1(2)}\exp\left[-i2\pi\left(k_{hY}^{(2)}y_0 + k_{hX}^{(2)}L\right)\right]\right|^2 \quad (5a)$$

and

$$P'_t(y_0) = \left|\Omega_{BL}\mathbf{D}_0^{1(1)}\exp\left[-i2\pi\left(k_{0Y}^{(1)}y_0 + k_{0X}^{(1)}L\right)\right] + \Omega_{BBL}\mathbf{D}_0^{1(2)}\exp\left[-i2\pi\left(k_{0Y}^{(2)}y_0 + k_{0X}^{(2)}L\right)\right]\right|^2. \quad (5b)$$

Here $k_{0Y}^{(j)}$ and $k_{hY}^{(j)}$ are the Y components of the wavevectors of the transmitted and diffracted beams, respectively, and $k_{0X}^{(j)}$ and $k_{hX}^{(j)}$ are the X components. Ω_{BL} and Ω_{BBL} are the correction factors of the beam widths for the corresponding diffractions in the BL and BBL cases (Authier, 2001; Yoshizawa *et al.*, 2008) and are given by

$$\Omega^2_{BL,\,BBL} = (l''/l_0) = (1 - r^2)/(1 + r^2). \quad (6)$$

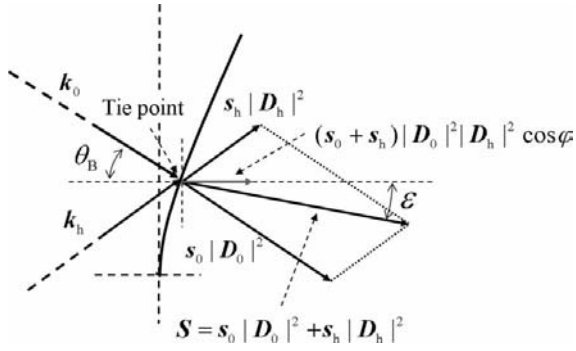

Figure 5
Schematic illustration showing the direction of the Poynting vector **S** with respect to the incident ($\mathbf{k}_0$) and the diffracted ($\mathbf{k}_h$) beams.

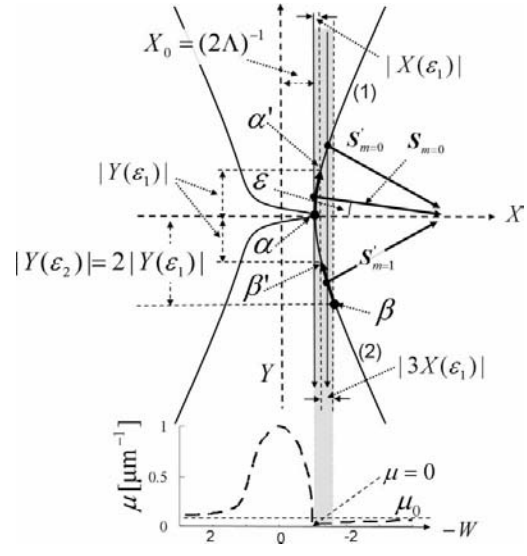

Figure 6
The dispersion surface and the Poynting vectors. The upper part shows the real part and the lower part the effective absorption coefficient μ (the imaginary part). The dispersion surface (1) lies on the upper side and the dispersion surface (2) on the lower side.

Here l_0 and l'' are the widths of the incident and the diffracted beams from the lateral surface as shown in Fig. 8. In this calculation, the beams in the multiple Bragg case ($m > 1$) are neglected because those beams are weaker than the beams in the BL and BBL cases.

Fig. 4 shows the calculated values of $P'_h(y)$ and $P'_t(y)$ by using the electric displacement fields $\mathbf{D}_{0,h}^{1(1)}$ and $\mathbf{D}_{0,h}^{1(2)}$ given in a previous paper (Hirano *et al.*, 2008). Although no phase shift in the x direction is taken into account in the previous paper, both phase shifts in the x and y directions are taken into account in Fig. 4 as described in §3.3. The peaks of the observed intensity distributions are well reproduced by the calculation except for the peak at $y = H$. The calculated fringes of $P'_h(y)$ and $P'_t(y)$ are in phase with each other, which is in good agreement with the measured results.

Since the relation $\mathbf{D}_h^{1(1)}(H) + \mathbf{D}_h^{1(2)}(H) = 0$ holds from the boundary condition, there should be no peak in $P'_h(y)$ at $y = H$. As the peak width of $P'_h(y)$ at $y = H$ is much narrower than those of the interference fringes and the peak height increases as L increases, the peak at $y = H$ cannot be explained by the interference effect but can be explained by the confined-beam effect, which comes from the third term in equation (1) (Fukamachi *et al.*, 2006). The beam confinement occurs because $\cos\varphi$ is not zero under the present experimental conditions.

3.3. Period of interference fringes

As described above, the fringes in Fig. 4 are caused by the interference between the internal waves excited by the incident beam in both the BL case and the BBL case. If we give the phase difference between the two beams in the x and y directions as $2\pi\Delta\theta_x$ and $2\pi\Delta\theta_y$, respectively, the total phase difference $2\pi\Delta\theta$ is given by

$$2\pi\Delta\theta = 2\pi(\Delta\theta_x + \Delta\theta_y) = 2\pi(\Delta x\Delta X + \Delta y\Delta Y). \quad (7)$$

Here Δx and Δy are the path differences in the x and y directions, and ΔX and ΔY are the differences in the X and Y components of the wavevectors in the reciprocal-lattice space.

In Fig. 7, the path of the beam in the BL case that reaches the point $y = 0$ on the lateral surface B is given as OQ, and that of the beam in the BBL case that reaches the point $y = 0$ is given as OP′Q, whose length corresponds to OP′Q″. The path difference between OQ and OP′Q in the y direction is $2H$. On the other hand, there is no path difference between two beams in the BL and BBL cases that reach the point $y = H$ (Q′). The path difference Δy between the beams reaching Q and Q′ is $2H$. The angle ε_2 in Fig. 7 is given by $\varepsilon_2 = \tan^{-1}(2H/L)$.

The beam propagating along OQ is excited at the point α on the dispersion surface (1) in Fig. 6 and the corresponding Poynting vector is $\mathbf{S}_{m=0}(\varepsilon = 0)$. The beam propagating along OP′Q is excited at the point β [$Y = -Y(\varepsilon_2)$] on the dispersion surface (2) and the corresponding Poynting vector is $\mathbf{S}'_{m=1}(\varepsilon = \varepsilon_2)$. The difference in the Y component of the wavevectors between two points α and β is $|Y(\varepsilon_2)|$ as shown in Fig. 6. There is no difference in the wavenumber between the two points α' [$Y = Y(\varepsilon_1)$] on the dispersion surface (1) and β' [$Y = -Y(\varepsilon_1)$] on the dispersion surface (2), because the beams from the tie points of α' and β' directly reach the point $y = H$ (Q′). Since the distance $|Y(\varepsilon_1)|$ between the points α and α' is the same as that of α and β', ΔY becomes $|Y(\varepsilon_2)|$ and the maximum phase angle $\Delta\theta_y^{\max}$ in the y direction is written as

$$\Delta\theta_y^{\max} = (\Delta y\Delta Y)_{\max} = 2H|Y(\varepsilon_2)|. \quad (8)$$

For a non-absorbing crystal, the equation of the dispersion surface is written as

$$X^2 = Y^2\tan^2\theta_B + X_0^2. \quad (9)$$

By differentiating equation (9) with respect to Y, the following relation is obtained:

$$X = \pm Y(\tan^2\theta_B/\tan\varepsilon) = \pm Y(\tan\theta_B/p), \quad (10)$$

where $\tan\varepsilon = \pm dX/dY$ and $p = \tan\varepsilon/\tan\theta_B$. By substituting equation (10) into equation (9), we obtain

$$Y(\varepsilon_2) = (H/\Lambda Lq\tan^2\theta_B), \quad (11)$$

with $q = [1 - p^2(\varepsilon_1)]^{1/2}$. As the difference in the path length Δx is L, the phase difference $\Delta\theta_x$ is given by $\Delta\theta_x = L\Delta X$. In the BL case, the distance between α and α' along the X direction is $\Delta X_{BL} = \Delta X(\varepsilon_1)$. In the BBL case, the distance between β' and β is $\Delta X_{BBL} = -3\Delta X(\varepsilon_1)$. The maximum difference in the wavenumber of ΔX becomes

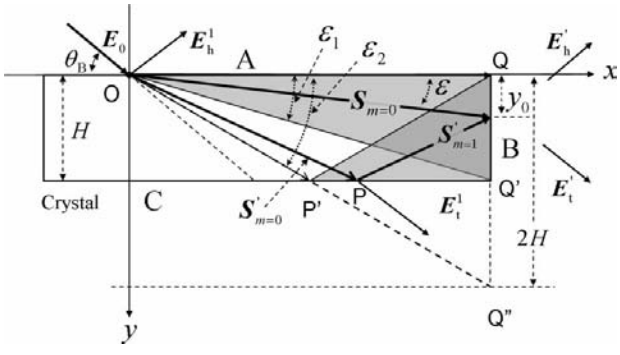

Figure 7
The paths of the beams in the BL and the BBL cases and the corresponding Poynting vectors $\mathbf{S}_{m=0}$, $\mathbf{S}'_{m=0}$ and $\mathbf{S}'_{m=1}$.

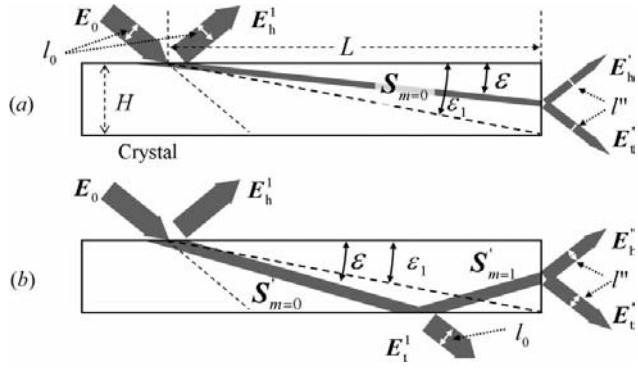

Figure 8
Illustrations of diffraction geometries for the determination of correction factors corresponding to the variations of the diffracted beam width. (*a*) BL case; (*b*) BBL case.

$$|\Delta X_{\max}| = |\Delta X_{\rm BL} + \Delta X_{\rm BBL}| = 2|\Delta X(\varepsilon_1)|. \quad (12)$$

When $\Delta\varepsilon = \varepsilon_1 - \varepsilon$, the difference in the X components of wavevectors in the BL and BBL cases is written as

$$\Delta X_{\rm BL\,or\,BBL}[\varepsilon_1(\mp)\Delta\varepsilon] = \Delta X(\varepsilon_1) - \Delta X(\varepsilon_1)[1(\mp)\delta]^2. \quad (13)$$

Here the upper sign in the parentheses is taken in the BL case and the lower sign in the BBL case. δ is zero at $y = H$ and 1 at $y = 0$. The difference in the wavenumber ΔX is obtained as

$$\Delta X = \Delta X_{\rm BBL}(\varepsilon_1 + \Delta\varepsilon) + \Delta X_{\rm BL}(\varepsilon_1 - \Delta\varepsilon) = -2\Delta X(\varepsilon_1)\delta^2. \quad (14)$$

By substituting $X(\varepsilon_1) = X_0 + \Delta X(\varepsilon_1)$ into equation (9), $\Delta X(\varepsilon_1)$ is given by

$$\Delta X(\varepsilon_1) = \Lambda Y^2(\varepsilon_1)\tan^2\theta_{\rm B}. \quad (15)$$

When $\delta = 1$, the maximum value $|\Delta\theta_x^{\max}|$ of the phase difference $\Delta\theta_x$ is obtained from equation (12) as

$$|\Delta\theta_x^{\max}| = |L\Delta X_{\max}| = |2L\Delta X(\varepsilon_1)| \quad (16)$$

and $|\Delta\theta_y^{\max}/\Delta\theta_x^{\max}| = 4q$. Using these relations, the phase shifts $\Delta\theta$, $\Delta\theta_y = 4HY(\varepsilon_1)\delta$, $\Delta\theta_x = L\Delta X$, $L\Delta X_{\rm BL}$ and $L\Delta X_{\rm BBL}$ normalized by $\Delta\theta_y^{\max}$ are calculated as a function of δ from 0 to 1 when $q = 1$. The results are shown in Fig. 9.

When $\Delta\theta_x + \Delta\theta_y = 1$, the period $\Lambda_{\rm B}(\delta) = \delta H$ is given as

$$\Lambda_{\rm B}(\delta) = \frac{\Lambda L}{2H}\frac{q}{[1 - \delta/(4q)]}\tan^2\theta_{\rm B} \quad (17)$$

because $2\Lambda_{\rm B}(\delta)Y(\varepsilon_2)[1 - \delta/(4q)] = 1$. $\Lambda_{\rm B}$ is proportional to L and is inversely proportional to H. Then it increases as y changes from H to 0. The calculated values of $\Lambda_{\rm B}$ obtained using equation (17) under the present experimental conditions agree with the measured results within the experimental error as shown in Table 1.

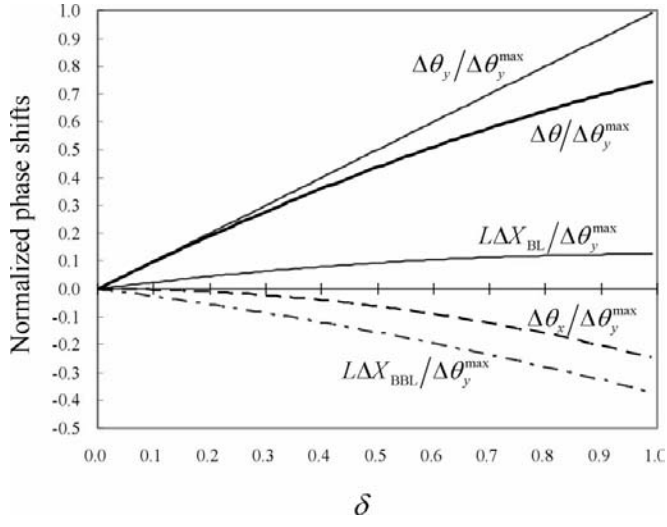

Figure 9
The phase shifts of $\Delta\theta$, $\Delta\theta_y = 4HY(\varepsilon_1)\delta$, $\Delta\theta_x = L\Delta X$, $L\Delta X_{\rm BL}$ and $L\Delta X_{\rm BBL}$ normalized by $\Delta\theta_y^{\max}$.

4. Summary

In summary, we have obtained the following results.

The interference fringes in the measured DLS are explained by the interference between the internal waves excited by the incident beam in both the BL case and the BBL case. The interference fringes in P_h' and $P_{\rm t}'$ are in phase with each other and the period of the fringes $\Lambda_{\rm B}$ is proportional to L and is inversely proportional to H according to equation (17). In addition $\Lambda_{\rm B}$ increases as y changes from H to 0.

The peak at $y = H$ cannot be explained by the interference fringe in the BB^{m}L case. According to the present analysis of the interference fringes in the BB^{m}L case, it is possible to observe the fringes from other samples such as Si. We have actually observed the fringes of the Si 220 reflection, but we could not observe the peak at the bottom end of the sample ($y = H$). This is because the absorption coefficient of Si is too small to cause the confined-beam effect. Detailed results will be published in a separate paper.

In this paper, as the incident X-ray energy was tuned very close to the Ge K-absorption edge, the beams in multiple Bragg cases ($m > 1$) can be neglected. But if the X-ray energy is about 10 eV below the Ge K-absorption edge, it is necessary to take the beams in multiple Bragg cases into account.

The present approach may be applied to the analysis of the interference fringes in the Laue–Bragg–Laue case, *i.e.*, the so-called Borrmann–Lehmann fringe (Borrmann & Lehmann, 1963; Lang *et al.*, 1986). As there was a large discrepancy between the periods of the interference fringes measured by Lang *et al.* (1986) and their calculated ones, it is necessary to measure the interference fringes more precisely by using the present experimental system.

When we could not measure DLS, we sometimes observed peaks from the mirage effect from the incident surface (Authier, 2001; Yan & Noyan, 2006). This in turn means that the DLS mode is very sensitive to lattice deformations due to defects in a perfect crystal, which is one of the useful applications of DLS.

The authors thank Professor Masayasu Tokonami of Saitama Institute of Technology and Professor Zhangcheng Xu of TEDA College, Nankai University for valuable discussions. They are grateful to Mr Toshiyuki Tanaka, Mr Tsuyoshi Oba and Mr Masahiko Tohyama for assistance in some experiments. This work was carried out under the approval of the Program Advisory Committee of PF (Proposal No. 2006-G274). This work was partly supported by the 'High-Tech Research Center' Project for Private Universities: 2004–2008 matching fund subsidy from MEXT (Ministry of Education, Culture, Sports, Science and Technology), and Grant-in-Aid for Scientific Research (C) (19540344) from MEXT.

References

Authier, A. (2001). *Dynamical Theory of X-ray Diffraction*, pp. 341–344. Oxford University Press.

Borrmann, G. & Lehmann, K. (1963). *Crystallography and Crystal Perfection*, edited by G. N. Ramachandran, pp. 101–108. London, New York: Academic Press.
Fukamachi, T., Negishi, R., Yoshizawa, M. & Kawamura, T. (2005). *Jpn. J. Appl. Phys.* **44**, L787–L789.
Fukamachi, T., Negishi, R., Yoshizawa, M. & Kawamura, T. (2006). *Jpn. J. Appl. Phys.* **45**, 2830–2832.
Fukamachi, T., Negishi, R., Yoshizawa, M., Sakamaki, T. & Kawamura, T. (2004). *Jpn. J. Appl. Phys.* **43**, L865–L867.
Hirano, K., Fukamachi, T., Yoshizawa, M., Negishi, R., Hirano, K., Xu, Z. & Kawamura, T. (2008). *J. Phys. Soc. Jpn*, **77**, 103707.
Lang, A. R., Kowalski, G., Makepeace, A. P. W. & Moore, M. (1986). *Acta Cryst.* A**42**, 501–510.
Pinsker, Z. G. (1978). *Dynamical Scattering of X-ray in Crystals*. Berlin, Heidelberg, New York: Springer Verlag.
Wagner, H. (1956). *Z. Phys.* **146**, 127–168.
Yan, H. & Noyan, I. C. (2005). *J. Appl. Phys.* **98**, 073527.
Yan, H. & Noyan, I. C. (2006). *J. Appl. Cryst.* **39**, 320–325.
Yoshizawa, M., Fukamachi, T., Hirano, K., Oba, T., Negishi, R., Hirano, K. & Kawamura, T. (2008). *Acta Cryst.* A**64**, 515–518.
Yoshizawa, M., Zhou, S., Negishi, R., Fukamachi, T. & Kawamura, T. (2005). *Acta Cryst.* A**61**, 553–556.